Photoactivation dynamics in photosynthetic and signal transduction proteins studied by ultra-fast time-resolved spectroscopy

Bonetti, C.

2009

document version
Publisher's PDF, also known as Version of record

Chapter 2

Identification of excited-state energy transfer and relaxation pathways in the peridinin-chlorophyll-*a* complex: an ultrafast mid-infrared study

Abbreviations: *A. carterae*, *Amphidinium carterae*; PCP, Peridinin Chlorophyll-*a* Protein; HSPCP, High-Salt PCP complex; Chl-*a*, Chlorophyll-*a* ; Per, Peridinin; (B)Chl, (Bacterio)Chlorophyll; LH, Light Harvesting; PSII, Photosynthetic System II; RC, Reaction Center; $CHCl_3$, Chloroform; MeOH, Methanol; CT, Charge Transfer; ICT, Intermolecular CT; S_2^*, second singlet excited state for peridinin; $^{hot}S_1^*$, vibrationally excited first singlet excited state for peridinin; $^{cold}S_1^*$, vibrationally relaxed first singlet excited state for peridinin; Q_y^*, first singlet excited state for Chlorophyll-*a*; ^{3}[Per]*, triplet excited state for peridinin; ^{3}[Chl-*a*]*, triplet excited state for chlorophyll-*a*; EET, Excitation Energy Transfer; TEET, Triplet EET; EADS, Evolution-Associated Difference Spectra; SADS, Specie-Associated Difference Spectra; DADS, Decay-Associated Difference Spectra; GSI, Ground State Intermediate; ESA, Excited State Absorption; IR, Infra-Red; TOPAS, Traveling-wave Optical Parametric Amplifier of Superfluorescence; NOPA, Non-collinear Optical Parametric Amplifier; MCT, Mercury-Cadmium-Tellurium; IRF, Instrument Response Function; FWHM, Full Width at Half Maximum; FID, Free Induction Decay.

[1]Bonetti C., [1]Alexandre M.T.A., van Stokkum I.H.M., Hiller R.G. , Groot M.L., Rienk van Grondelle, and John T.M. Kennis

Manuscript in Preparation

[1]*Authors contribute equally to the work*

Abstract

Peridinin Chlorophyll-*a* Protein (PCP) is a water soluble Light Harvesting Complex found in the dinoflagellate, *Amphidinium carterae*. In the high-resolution X-ray structure (2 Å) PCP appears as a trimer of polypeptides. Each polypeptide monomer can be divided into two quasi-symmetric sub-units containing one Chlorophyll-*a* (Chl-*a*) closely surrounded by 4 Peridinin (Per). In this paper the dynamics of Per dissolved in organic solvent ($CHCl_3$ and MeOH) and of Chl-*a* and Per in PCP were studied using time-resolved femtosecond visible-pump mid-infrared probe spectroscopy. For Per in solution the IR signatures of the S_1 and ICT are similar, in line with a previous ultrafast IR study. In PCP, excitation of Chl-*a* reveals two *9*-keto modes at 1699 and 1687 cm^{-1} that upshift in the singlet excited state. In addition, *10a*-ester vibrations are observed at 1736 and 1727 cm^{-1}. The Per and Chl-*a* molecules were selectively excited at two different wavelengths, 480 nm for the Per and 660 nm for the Chl-*a*. Excitation of the Chl-*a* at 660 nm reveals a vibrational cooling process in 200 fs. The Chl-*a* singlet excited-state has a lifetime of ≈ 3 ns, and evolves into the Per triplet with this time constant, indicating that Chl-Per triplet energy transfer is significantly faster. Following 480 nm excitation, an ultrafast decay component is identified ($S_2 \rightarrow S_1$ and $S_2 \rightarrow$Chl-*a*) followed either by a fast energy transfer from the $^{hot}S_1^*$ energy state of Per to Chl-*a* or by vibrational relaxation from $^{hot}S_1^*$ to S_1^* (150 fs). Target analysis distinguishes two separate low-lying singlet excited states, assigned to ICT state which transfers to Chl-*a* in 2 ps and a vibrationally relaxed S_1 state, which slowly transfers to Chl-*a* in ~30 ps. The ICT and S_1 state have their lactone bleach at 1745 and 1749 cm^{-1} respectively, indicating that separate peridinins carry the ICT and S_1 state. From the Chl-*a* singlet excited state, efficient triplet excitation energy transfer (TEET) takes place to Per as no Chl-*a* triplet is observed, but rather a direct formation of Per triplet. The latter contains some Chl-*a* features due to strong coupling of the pigments. The Per triplet spectrum shows a lactone bleach at 1749 cm^{-1}, indicating that the triplet accepting Per is distinct from that carrying the ICT state. On the basis of the ultrafast IR data, the Per excited states involved in energy transfer and relaxation can be related with transient population of

particular peridinins, i.e., S_1 localizes on Per622/612, ICT on Per621/611 and Per623/613 and the Per triplet state on Per624/614.

Introduction

Photosynthesis is the main process that supports life on Earth. It converts the most abundant energy source on the planet, solar energy, into chemical energy, which is used by nearly all organisms. The pigment-protein complexes that constitute the photosynthetic apparatus are highly evolved to cover the biodiversity of the hosting organisms and to fit requirements imposed by the environment. The complexes that function to harvest sunlight are called light harvesting antennas. The light harvesting pigments differ among organisms; in the majority of the complexes, (bacterio)chlorophylls ((B)Chl) and carotenoids constitute the main chromophores. How the (B)Chls harvest light is reasonably well-understood [1, 2]; however, many questions remain on the role of carotenoids in LH complexes and their interaction with the (B)Chl due to their complex excited state levels and the different functions assumed by these pigments [3-6]

Oceanic photosynthetic organisms contribute largely to the global CO_2 fixation [7], and their LH apparatus has evolved to absorb light at higher frequencies compared with land-based photosynthetic organisms. The reason to shift the absorption towards the blue lies in the increased absorption by water of red light compared to blue; such aquatic organisms are illuminated by light that has a relatively high intensity in the blue and the green, and consequently the pigments in their LH complexes must absorb at higher frequencies. Red algae, cryptophytes and cyanobacteria developed phycobilisome light harvesting complexes with open-chain tetrapyrrole pigments [8]. In eukaryotic marine algae, carotenoids play the role of major light harvesting pigments [9]

Amphidinium carterae is a most interesting oceanic photosynthetic algae and belongs to the family of dinoflagellates; this eukaryotic algae uses a water-soluble Peridinin-chlorophyll-*a* protein (PCP), a trimeric light harvesting antenna that binds the carotenoid peridinin and Chl-*a* in an unusual stoichiometric ratio of 4:1. PCP harvests sunlight and transfers energy to the photosystem II (PSII) reaction center (RC) core [10, 11]. The X-ray structure of PCP, shown in Figure 1, revealed that

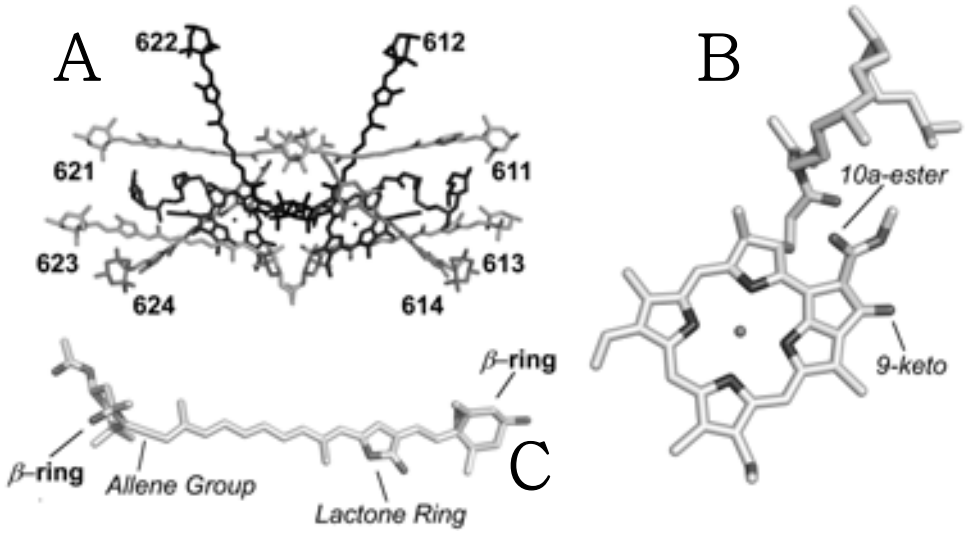

Figure 1: A, Arrangement of pigments in PCP monomer. Numbers refer to the peridinin notation based on PDB entry 1PPR (ref. [12]); **B**, Molecular structure of Peridinin. The two β – and one lactone– rings and the allene group are shown; **C**, Molecular structure of Chlorophyll-*a*. *9*-keto and *10a*-ester carbonyl groups are evidenced.

each monomer is divided into two quasi-symmetric subunits containing one Chl-*a* closely surrounded by four Per [12]. Generally, the EET efficiency from carotenoids to (B)Chl can vary from <30% to almost 100% [6, 13, 14]. Per are excellent light harvesters that have a strong absorption in the green from 480 to 530 nm when bound to PCP and achieve a high efficiency of excitation energy transfer (EET) to Chl-*a* of ~90%. The remarkable efficiency is proposed to result from the tight packing of the pigments as well as a peculiar excited state manifold of peridinin [15-17]. Such chromophore organization is also responsible of a highly efficient Chl-*a* triplet quenching of 100% [15, 18]. Besides the distance and orientation separating the pigments, the EET efficiency is directly related to the carotenoid excited state manifold responsible for the mechanisms and pathways of EET. For peridinin, stabilization of an intramolecular charge-transfer (ICT) state is held responsible for such a high efficiency [16, 19-21].

Peridinin is the most highly substituted Car known in nature. It has an unusually short carbon skeleton (C_{37}), an allene group and a lactone ring both conjugated with the backbone (Figure 1). At both ends of the conjugated carbon chain, two β-rings are located with an epoxy group with a secondary alcohol group, and an ester group located on the

opposite β-ring with a tertiary alcohol group. After excitation of peridinin, the relaxation pathway from the strongly absorbing $1Bu^+$ state (S_2) depends strongly on the polarity of the environment [19, 22-25]. In the nonpolar solvent hexane, S_2 rapidly internally converts to the $2Ag^-$ (S_1) state, which has a 160 ps lifetime, as expected for a carotenoid with eight conjugated double bonds [19]. However, in polar solvents (e.g. methanol and ethylene glycol), the excited state lifetime was found to be ~10 ps [19, 23, 25]. It was suggested that this acceleration was due to the stabilization of a low-lying ICT state in polar solvent that is energetically lower than S_1 [22, 24] and involves a structural rearrangement [24]. Papagiannakis *et al* [23] resolved the excited state equilibrium between S_1 and ICT state in solution demonstrating that they are distinct states. In addition, observation of a ground state intermediate (GSI) on the relaxation pathway sustains the hypothesis that population of the ICT state may stabilize a small-scale structural rearrangement of Per.

In PCP, peridinin employs multiple energy transfer channels to achieve a high efficiency. Upon excitation of the S_2 state, 25% of its energy flows to Chl-*a* directly [16, 21]. Peridinins in PCP are bound in a rather polar environment which favors population of the ICT state after excitation [21]. The major channel of energy transfer in PCP is on the timescale of about 2 ps and involves the ICT states [15, 16, 21]. Recently, non-linear polarization spectroscopy experiments on PCP confirmed that ICT is isoenergetic or slightly above Q_y of Chl-*a* [26]. The PCP complex therefore represents an example of a system where energy-transfer pathways and their efficiencies are finely tuned not only by the protein structure ensuring a proper orientation of the donor and acceptor molecules, but also by the polarity and/or hydrogen-bonding capability of the environment adjusting the degree of charge-transfer character of the lowest excited state.

The vibrational spectrum of a protein or a protein-bound chromophore contains a wealth of information about its structure, the interaction with the environment and electronic properties. Time-resolved IR spectroscopy is a powerful tool that can reveal many of the dynamic structural and physical-chemical properties of chromophores involved in (photo)biological reactions [27, 28]. It has revealed energy and electron transfer pathways in photosynthetic antennae and reaction centers [29-34] and given detailed insight into reaction dynamics of biological photoreceptors [35-40].

In this work, the excited-state energy transfer and relaxation pathways in PCP were studied using ultrafast visible-pump mid-IR probe spectroscopy. We determined the IR signature of the various peridinin and Chl-*a* molecular states involved in energy transfer processes, in particular those of the peridinin S_1, ICT and triplet states. By comparing the frequencies of the peridinin lactone modes of these states, we identified the involvement of particular peridinins to specific events in the light-harvesting process.

Materials and Methods

Sample Preparation

Samples of PCP from *A. carterae* were purified as described in [12] and dissolved in D_2O buffer (25 mM TRIS Cl, 2 mM KCl, 3 mM NaN_3, pD= 7.5). Per was isolated from *A. carterae* thylakoids by the method of Martison and Plumley [41] and was purified using reverse phase HPLC using an Alltech C18 column. The sample were concentrated to OD_{480}= 0.6/20 μm and OD_{660}= 0.4/20 μm (for PCP) and OD_{530}= 0.4/5 μm (for Per in solution) placed in a sample cell formed by two CaF_2 plates separated by a 20 μm (5 μm) Teflon spacer for a total volume of 40 μL (10 μL). To avoid photodamage during the measurements, the sample was continuously moved by a home-built Lissajous scanner.

Experimental Setup

The experimental setup, described in detail previously [30] consists of a Ti:sapphire amplified laser system (Hurricane, Spectra-Physics) providing a 800 nm source, with an output of 0.65 mJ, repetition rate at 1 kHz and duration of 85 fs. A portion of the 800 nm light was used to pump an optical parametric generator and amplifier with difference frequency generator (TOPAS, Light Conversion, Vilnius, Lithuania), producing tunable output (2.5 – 10 μm) with a bandwidth of ~ 200 cm^{-1}. The probe pulse on the sample was attenuated to 1 nJ. A second portion of the 800 nm light was sent into a home-built non-collinear optical parametric amplifier (NOPA) to produce the pump pulse at 480 nm

(660 nm) with a power of 75 nJ (150 nJ), which was used to excite the sample. The polarization between pump and probe pulses was set at the magic angle (54.7 °) using a Berek rotator (Model 5540; New Focus, San Jose, CA). The probe pulse was collimated and focused on the entrance slit of a spectrograph and dispersed onto a 32-element mercury-cadmium-tellurium (MCT) detector array, yielding a spectral resolution of 4 cm^{-1}. The instrument response function (IRF) of the system had a width of 150 fs (FWHM). Changes in the IR absorption were monitored in the carbonyl region from 1780 to 1650 cm^{-1} in a time range of six nanoseconds.

Data Analysis

The time-resolved data can be described in terms of a parametric model in which some parameters, such as those descriptive of the instrument response function (IRF), are wavenumber-dependent, whereas others, such as the lifetime of a certain spectrally-distinct component, underlay the data at all wavenumbers. The presence of parameters that underlay the data at all wavenumbers allow the application of global analysis techniques [42], which model wavenumber-invariant parameters as a function of all data. The partitioned variable projection algorithm is well-suited to the optimization of model parameters for global analysis models [43]. The algorithm has the further advantage of estimating the standard error of parameter estimates, an advantage that is useful in model selection and validation. A compartmental model was used to describe the evolution of the spectrally distinct components in time. Global analysis was then applied to estimate the lifetime and relative concentration of each component at each wavenumber in the data.

The femtosecond transient absorption data were first globally analyzed using a kinetic model consisting of sequentially interconverting evolution-associated difference spectra (EADS), i.e. $1\rightarrow2\rightarrow3\rightarrow...$ (Figure 2, 3 and 5A) in which the arrows indicate successive mono-exponential decays of increasing time constants, which can be regarded as the lifetime of each EADS. The first EADS corresponds to the time-zero difference spectrum. This procedure enables us to clearly visualize the evolution of the (excited and intermediate) states of the system. In general, the EADS may well reflect mixtures of molecular states.

To disentangle the contributions by the various molecular species in the spectral evolution, we performed a target analysis of time-resolved data. Target analysis involves the application of a compartmental model (insert in Figure 6) containing microscopic decay rates expressing intercompartmental transitions, and may be used to test detailed hypotheses regarding the underlying kinetics. The spectrum associated with each component in a target analysis applied to difference absorption data is termed species-associated difference spectrum (SADS, Figure 6). In contrast to the EADS, the SADS will represent the spectral signature of the pure molecular species and their kinetics after photon absorption. In this way, energy transfer and relaxation pathways and mechanisms can be assessed in terms of discrete intermediate states.

Results

Here, we describe the results of an ultrafast visible pump, mid-infrared probe spectroscopic study on PCP and peridinin in solution to characterize the energy transfer and relaxation pathways and mechanisms on the fs to ns timescale. Two excitation wavelengths were used, 660 nm and 480 nm, resonant with the Q_y transition of the Chl-*a* molecules and the maximum of peridinin absorption, respectively.

Peridinin in solution

The excited-state dynamics of peridinin in organic solvent were studied to aid the interpretation of peridinin dynamics in the PCP complex. Figure 2A shows the EADS for peridinin in chloroform ($CHCl_3$) upon excitation at 530 nm. Five components were required for a satisfactory fit of the time-resolved data, with lifetimes of 100 fs, 1.7 ps, 6.6 ps, 65 ps and a nondecaying component. The first EADS with a 100 fs lifetime (light gray dashed line, 1) corresponds to the initially excited S_2 state that internally converts to the optically forbidden S_1 state. Note that this EADS may be affected by the perturbed FID and therefore cannot be reliably interpreted. The following EADS with lifetimes of 1.7 ps, 6.6 ps and 65 ps represent the optically forbidden S_1 state of peridinin. These EADS have very similar shapes with an overall broad, nonspecific induced

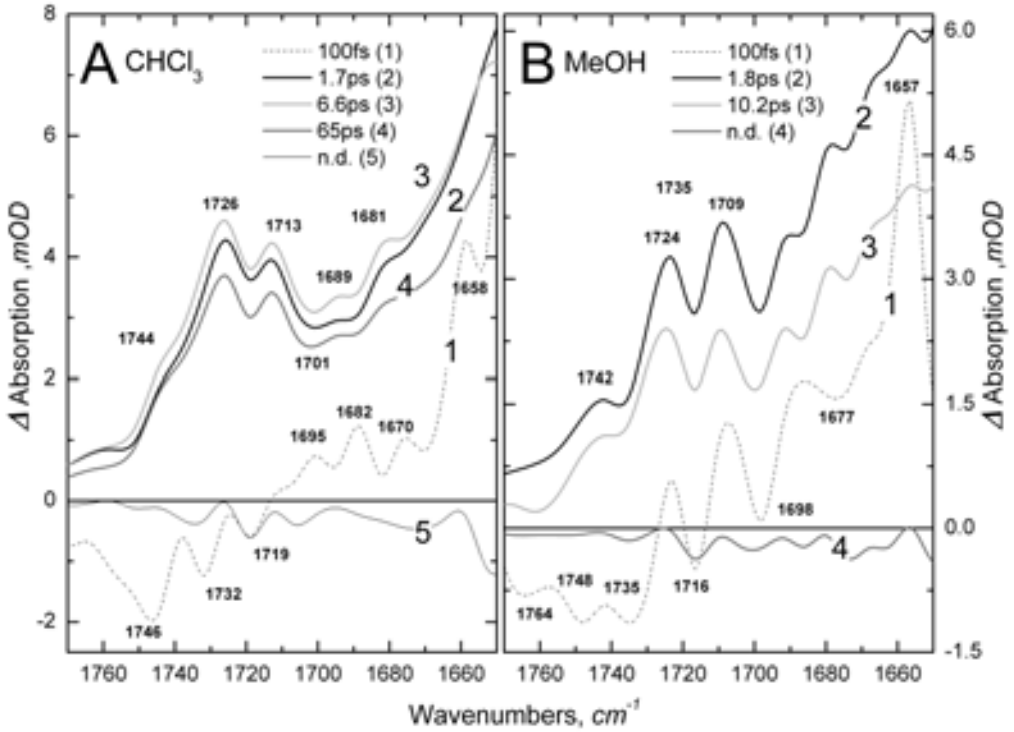

Figure 2: EADS, evolution-associated difference spectrum, resulting from Global Analysis on Peridinin in: **A**, $CHCl_3$ and **B**, MeOH after 530 nm excitation with an energy of 100 nJ per pulse.

absorption with a superimposed pattern of ground state bleach and induced absorptions. Due to the overall positive amplitude of the EADS it is difficult to identify the exact bleach/induced absorption frequencies. The IR difference spectra are similar to those reported previously for peridinin in solution [44], except that in the latter case, a slight spectral evolution was observed with relative amplitude changes of the bands. The 1.7 and 6.6 ps evolutions represent only minor spectral and amplitude changes and may be associated with vibrational cooling and solvation processes, possibly in combination with charge-transfer equilibration [23]. The S_1 signal decays to essentially zero in 65 ps, in line with the ultrafast IR study on peridinin reported by Van Tassle et al. [44] and peridinin lifetimes reported for nonpolar solvents [19].

Figure 2B shows the EADS for peridinin in MeOH. Three components were required for an adequate fit, with time constants of 100 fs, 1.8 ps and 10 ps. The overall spectral shape of the EADS is similar

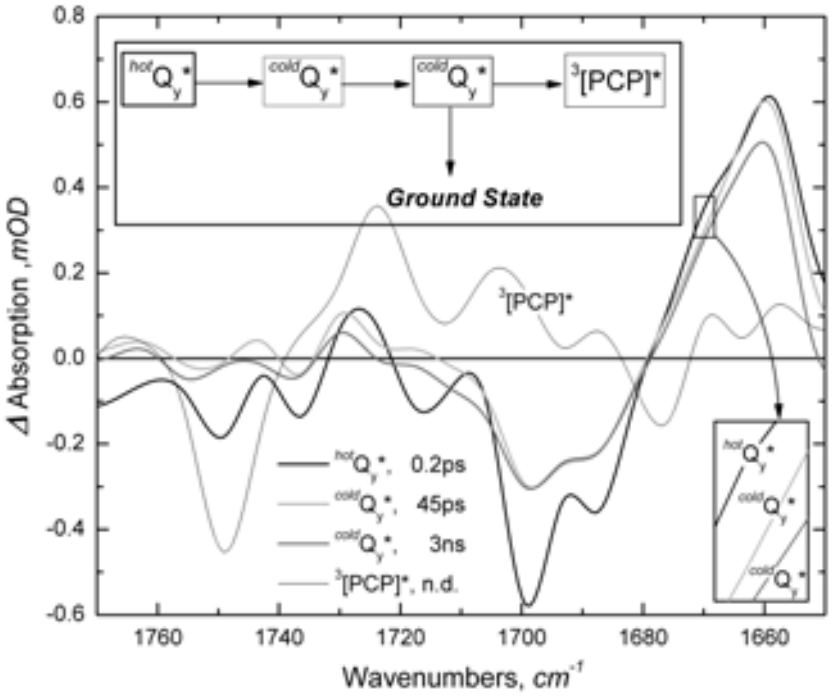

Figure 3: SADS, Species-associated difference spectrum, resulting from Global analysis on PCP in D_2O after exciting the Q_y band of Chl-*a* at 660 nm with an energy of 150 nJ per pulse. In the insert is reported the sequential scheme used for the analysis. In the insert is drew the sequential scheme used for the analysis.

to those observed earlier for peridinin in d4-MeOH [44]. Also, the EADS of peridinin in methanol and in chloroform (Figure 2A) are not much different, implying that the mid-IR signatures of the optically forbidden peridinin S_1 and ICT states are rather similar, confirming Van Tassle *et al* [44].

Chlorophyll-a excitation of PCP: Global analysis

PCP in D_2O buffer was excited at 660 nm to determine the Chl-*a* dynamics upon direct excitation. A spectral window between 1770-1650 cm^{-1} was probed. Figure 3 shows the result of a global analysis in terms of a sequential kinetic scheme (Figure 3, inset) in the form of evolution-associated difference spectra (EADS). Kinetic traces at selected frequencies are shown in Figure 4. Four components were required for

an adequate description of the time-resolved data. For this excitation wavelength the spectra resulting from a sequential analysis are associated to molecular species due to the sequential nature of the energy relaxation process, and may be regarded as species-associated difference spectra (SADS).

The first component (Figure 3, bold black line) is formed within the instrument response (150 fs) and decays in 200 fs into the second component (Figure 3, light gray). The second component evolves in 45 ps into a third component (dark gray), which decays in 3 ns to form a non-decaying species (Figure 3, thin black line). The concentration profiles associated with each species are shown in Figure A in *Appendix*, along with the IRF.

The first EADS (Figure 3, bold black line) exhibits bands at 1699(-), 1687(-), 1670(+, shoulder) and 1658(+) cm^{-1}, assigned to the

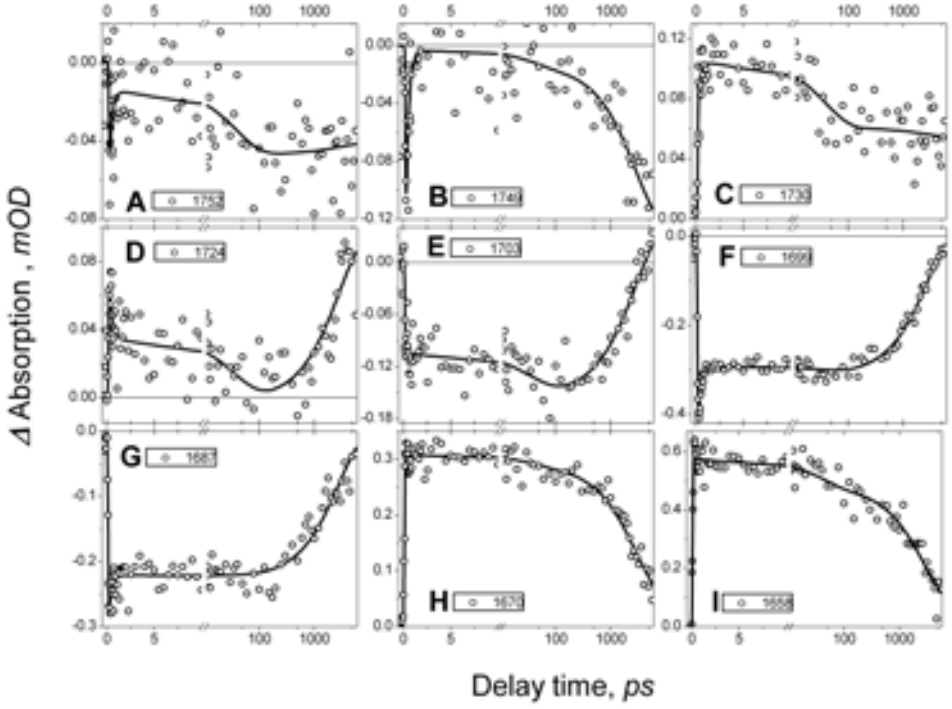

Figure 4: Nine selected time traces relative to the 660 nm data are reported. The time axis is linear between zero and ten picoseconds and logarithmic thereafter.

9-keto modes of the two Chl-*a* in the asymmetric subunit [45] (Figure 4, traces F,G, H, and I). The vibrational mode frequencies and their assignments are summarized in Table 1. In addition, it shows bands at 1736(-) and1727(+) cm^{-1} assigned to *10a*-ester carbonyl stretches of Chl-*a*. These assignments are in good agreement with earlier reports [29, 30, 46].

Table 1 Spectral positions and assignments of the observed vibratonal bands in the SADS that follow from global analysis on femtosecond time-resolved transient absorption data of PCP domain after exciting the Chl-*a* with a 660nm

$^{hot}Q_y$*	$^{cold}Q_y$* $^{cold}Q_y$*(Eq)	^{3}[PCP]	
	1752(-)		
1750(-)	1743(+)	1749(-)	*10a*-ester Lactone(Per)
1736(-)	1736(-)		
1727(+)	1730(+)		*10a*-ester Lactone(Per)
		1724(+)	Lactone(Per)
1718(-)		1703(+)	Lactone(Per)
1699(-)		1693(-)	
1670(+ sh)	1699(-)	1670(+)	*9a*-keto
1687(-)	1687(-)	1677(-)	
1658(+)	1658(+)	1658(+)	*9a*-keto

Interestingly, The first EADS also contains a negative band at 1718 cm^{-1}, which may be assigned to a C=O lactone stretch of peridinin [47]. Thus, the first EADS exhibits explicit Peridinin contributions which may be indicative of exciton coupling between Chl-*a* and peridinin. We note, however, that some caution should be taken when interpreting this EADS given that perturbed free induction decay (FID) signals may contribute at such short timescales [48].

The first EADS relaxes in 200 fs into the 2nd EADS (light gray line). The 2nd EADS clearly shows the presence of two distinct *9*-ketos stretches at 1699(-)/1687(-)/1658(+) cm^{-1} and two distinct *10a*-ester stretches at 1752(-)/1743(+) cm^{-1} (Figure 4, trace A) and 1736(-)/ 1730(+) cm^{-1}(Figure 4, trace C), assigned to the two Chl-*a* bound within the PCP monomer. Notably, the peridinin contribution (1718 cm^{-1}) is much weaker. With the black to red evolution, an overall shift of the

Chl-*a* ESA towards higher wavenumbers is observed: the *10a*-ester ESA shifts from 1727 to 1730 cm^{-1} and the *9*-keto ESA becomes sharper. These are fingerprints for vibrational cooling, so we identify the first EADS (bold black line) as $^{hot}Q_y^*$ which relaxes in 200 fs to a vibrationally relaxed Q_y (light gray EADS). Again, perturbed free induction decay (FID) signals may contribute at such short timescales so caution should be taken. The second EADS decays in 45 ps in the dark gray EADS and represents a relatively minor spectral evolution.

The third EADS has a lifetime of 3 ns, which is typical for the singlet excited state of Chl-*a* in PCP [18, 21]. The nondecaying EADS (thin black line in Figure 3) is difficult to estimate due to its low amplitude and the relatively poor signal-to-noise in the experiments. Nevertheless, the prominent negative feature at 1749 cm^{-1} and a broad ESA at 1724 cm^{-1} (Figure 4, trace D) may be assigned to a downshift of the peridinin C=O lactone stretch vibration, as observed in the peridinin triplet state ^{3}[Per]* [47]. Thus, the peridinin lactone signal rising at long delay times (Figure 2, trace B), assigned to the Per triplet state (^{3}[Per]*) is formed upon TEET from ^{3}[Chl-*a*]*. Note that the peridinin triplet state is rising faster than with the 17 ns time constant reported previously [15]. Such fast rise of the carotenoid triplet state, without observable ^{3}[Chl-*a*]* intermediate was observed in bacterial and artificial LH complexes as well [49-51].

Peridinin excitation of PCP at 480nm: Global analysis

PCP in D_2O buffer was excited at 480 nm to determine the infrared signature of the peridinin to Chl-*a* energy transfer dynamics. The EADS that follow from a global analysis, using a sequential model are shown in Figure 5A. Six components were required to satisfactorily fit the data, with time constants of 60 fs, 150 fs, 2 ps, 11.5 ps, 1 ns and a non-decaying component. The sequential scheme used for the analysis is shown in the inset of Figure 5A, the concentration profiles associated with each EADS are reported in Figure B in *Appendix* together with the IRF. The time constants are similar to those found with ultrafast spectroscopy in the visible and near-IR [16, 20, 52, 53].

The first EADS (black dashed line in Figure 5A), appears instantaneously (within the IRF), and decays in ~60 fs into the second

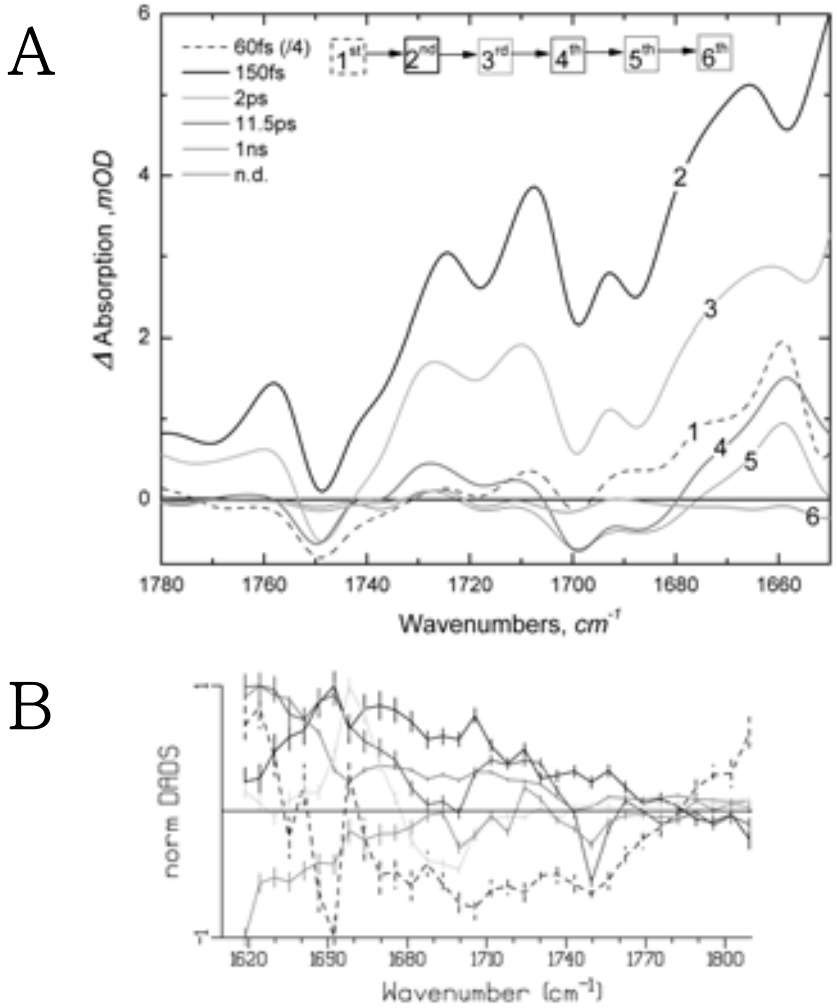

Figure 5: A, EADS, evolution-associated difference spectrum, resulting from Global analysis on PCP in D_2O after 480 nm excitation with an energy of 75 nJ per pulse. In the insert is drew the sequential scheme used for the analysis. **B**, DADS, decay-associated difference spectrum, resulting from Global analysis on PCP in D_2O after 480 nm excitation with an energy of 75 nJ per pulse. Key as in legend Figure 5A; vertical bars indicate estimated standards errors.

EADS. Even if the IRF is adequate to measure such a fast process (see comparison between IRF and ultrafast component concentration profile in Figure B), the estimated spectrum is highly uncertain due to its mixing with perturbed FID signals [48]. This uncertainty limits the interpretation

of this component to its lifetime and kinetic connectivity with the other components.

The second EADS (Figure 5A, bold black line) has a lifetime of 150 fs. It shows a broad ESA (absorption) all across the spectrum, indicating peridinin excited states (cf. the results on peridinin in solution). On top of the broad ESA, bands are identified at 1770(−)/1758(+) cm^{-1}, 1749(−)/1724(+) cm^{-1}, 1718(−)/1708(+) cm^{-1}. All these bands can be assigned to peridinin. Considering the broad, nonspecific absorption of the lowest peridinin excited states, the positive band maxima given here should be considered as tentative. Besides the peridinin signals, Chl-*a* modes are also observable at 1699 and 1687 cm^{-1}. The associated ESA appears as a broad band at 1666 cm^{-1} with a shoulder at 1676 cm^{-1}. The third EADS (light gray line) is formed in 150 fs and has a lifetime of 2 ps. It retains the features of the 2^{nd} EADS, indicating that the two EADS describe electronic states that are closely related. In the 3^{rd} EADS, the ESA are slightly blue shifted from 1724 and 1708 cm^{-1} to 1727 and 1710 cm^{-1}, indicating a vibrational cooling process.

The 4^{th} EADS (dark gray line) rises in 2 ps and has a lifetime of 11.5 ps. The 2 ps evolution from the previous EADS is accompanied by major spectral changes. The positive ESA (absorption) that was dominating the previous EADS (spectra 2 and 3, in Figure 5A) has disappeared. The Chl-*a* bleach bands are now strongly present at 1699(−) and 1687(−)cm^{-1}, the associated ESA is found at 1658 cm^{-1}, in agreement with the results shown in Figure 3. A 2 ps lifetime is typically associated with that of the peridinin ICT state in PCP [16, 19-21].

The evolution to thr 5^{th} EADS (thin black line) in 11.5 ps represents multiple processes, which can be understood from inspection of the normalized DADS in Figure 5B. The 11.5 ps DADS can be regarded as a superposition of Chl-*a* decay (1687 cm^{-1} and 1699 cm^{-1} bands) due to Chl-*a* singlet-singlet annihilation and decay of the slowly transferring Per S_1 state (ESA below 1720 cm^{-1} and bleach at 1745 cm^{-1}) [53]. The 1749 cm^{-1} band loses a major part of its intensity and a new band appears at 1736(−)/1730(+) cm^{-1} assigned to an ester stretch of Chl-*a* in agreement with the results shown in Figure 3. The 5^{th} EADS (thin black line) rises in 11.5 ps and has a lifetime of 1 ns, it is characterized by a decay time of 1 ns, compatible with the decay time of the Q_y singlet excited state of Chl-*a* in PCP, and contains Chl-*a* features together with peridinin modes at 1717(−) and 1749(−) cm^{-1}. The thin black EADS

decays into the final, nondecaying EADS (tick light gray, line 6), which is characterized by a strong band at 1749(-)/1725(+) $cm^{-1}$and weaker bands at 1718(-)/1711(+) cm^{-1} and 1699(-) cm^{-1} assigned to two different lactone C=O conformers and a keto stretch of Chl-*a* respectively. This nondecaying EADS is formed via TEET from Chl-*a* to peridinin and is assigned to the peridinin triplet state.

Peridinin excitation of PCP at 480nm: Target analysis

The EADS that emerge from the global analysis in terms of a sequential model are rather complicated and difficult to interpret as vibrational features of both chromophores are present in each spectrum. This follows from the previously observed fact that after excitation in the peridinin S_2 state, a rapid branching occurs in less than 100 fs with excited-state energy flowing into low-lying peridinin states in competition with energy transfer to Chl-*a*. To properly understand the molecular basis of energy transfer and relaxation in PCP, the spectroscopic signature of each individual state involved in these processes must be determined. In particular, it is anticipated that the mid-IR signatures of the various molecular states will yield information previously not revealed by visible/near IR spectroscopy. To disentangle the contributions by each molecular state to the spectral evolution, we have applied a target analysis to the data with peridinin excitation at 480 nm using a kinetic model based on earlier ultrafast UV-visible data [53]. The inset of Figure 6 (see also Figure C in *Appendix*)shows the kinetic scheme to describe the PCP dynamics, consisting of 6 molecular states. After excitation of the peridinin S_2^* state (dashed line), energy transfer takes place to Chl-*a* (thin black line, denoted as Q_y^*) in competition with internal conversion to a hot peridinin S_1^* state (bold black line) [16, 21, 53]. From the $^{hot}S_1^*$ state, further energy relaxation takes place to a vibrationally relaxed S_1 state (thin dark gray, denoted as $^{cold}S_1^*$) and an intramolecular ICT state (bold light gray line). From the ICT state, energy transfer takes place to Chl-*a*. The vibrationally relaxed S_1 state transfers energy to Chl-*a* and internally converts to the ground state. Finally, Chl-*a* partly relaxes to the ground state and undergoes intersystem crossing to the triplet state (bold dark gray line, denoted as ^{3}[PCP]*). The yields and rate constants are reported in *Appendix* in Figure D. Each state

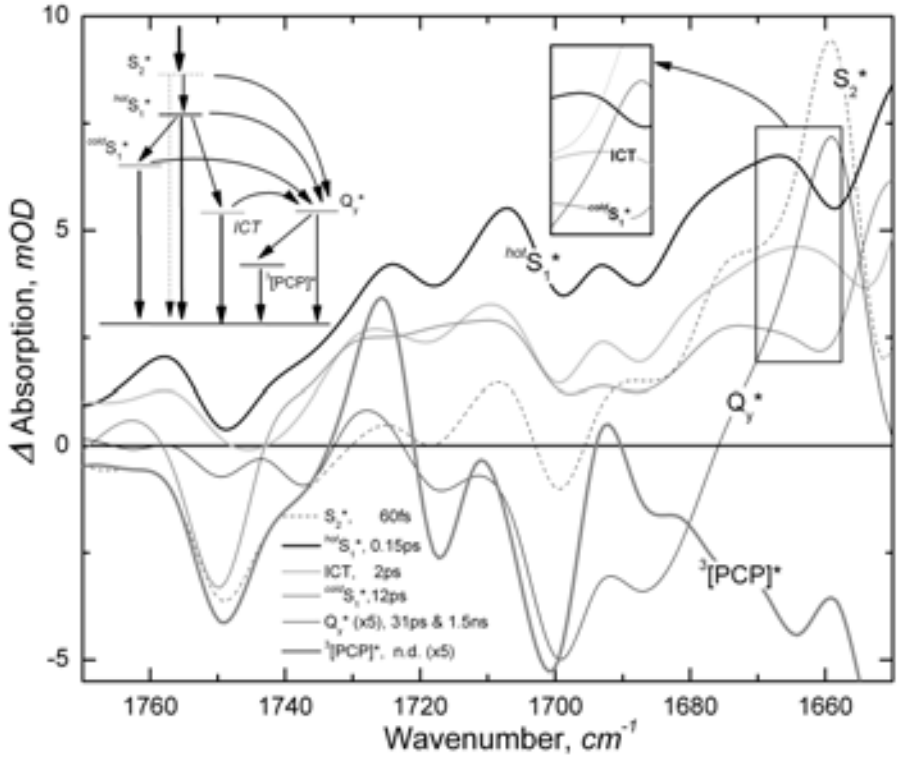

Figure 6: SADS, species-associated difference spectrum, resulting from Target analysis on PCP in D_2O after exciting the Peridinins at 480 nm with an energy of 75 nJ per pulse. The dynamic of the SADS is shown by color evolution: Black-dashed, Black, Red, Blue, Green, Magenta. SADS green and magenta have been magnified five folds for a better visualization and comparison. Scaling factors are reported in brackets. Kinetic model applied for the analysis is drew in the figure.

corresponds a species-associated difference spectrum (SADS), displayed in Figure 6. Some spectra have been rescaled to allow better comparison (scaling factors are reported in the caption of Figure 6). Kinetic traces at selected vibrational frequencies are reported in Figure 7. Concentration profiles associated with the SADS are shown in Figure C in *Appendix*. Upon excitation, the optically allowed S_2 state of peridinin decays in about 60 fs, populating the $^{hot}S_1^*$ and Chl-*a*. The lifetime of this component is consistent with the 66 fs lifetime found for Per S_2 in PCP by fluorescence up-conversion [54]. The SADS of the S_2 state shows a high similarity with the first EADS observed in similar experiments on Peridinin dissolved in $CHCl_3$ and MeOH, Figure 2A and 2B. It should be noted, however, that at these early time delays, effects from the

perturbed FID may strongly affect the spectra, and therefore we refrain from further physical interpretation.

The Chl-*a* compartment is populated by energy transfer from the carotenoid through S_2^*, $^{hot}S_1^*$ and ICT, and follows a bi-exponential decay with characteristic lifetimes of 31 ps and 1.5 ns. The first phase of 31 ps describes energy redistribution and annihilation between different Chl-*a* inside the same trimer [18], in agreement with the 45 ps lifetime found with 660 nm excitation. After energy redistribution, the excited Chl-*a* decays in 1.5 ns to the ground state for 70%, and to form the non-decaying component with a yield of 30% by intersystem crossing and TEET (^{3}[PCP]* spectrum in Figure 6). The Chl-*a* SADS is similar to that observed with direct excitation at 660 nm (Figure 3) but better resolved as a result of a superior signal to noise ratio. It shows the *9*-ketos at 1699(-),1687(-)/1659(+) cm^{-1} (Figure 7F, H and I), and the two

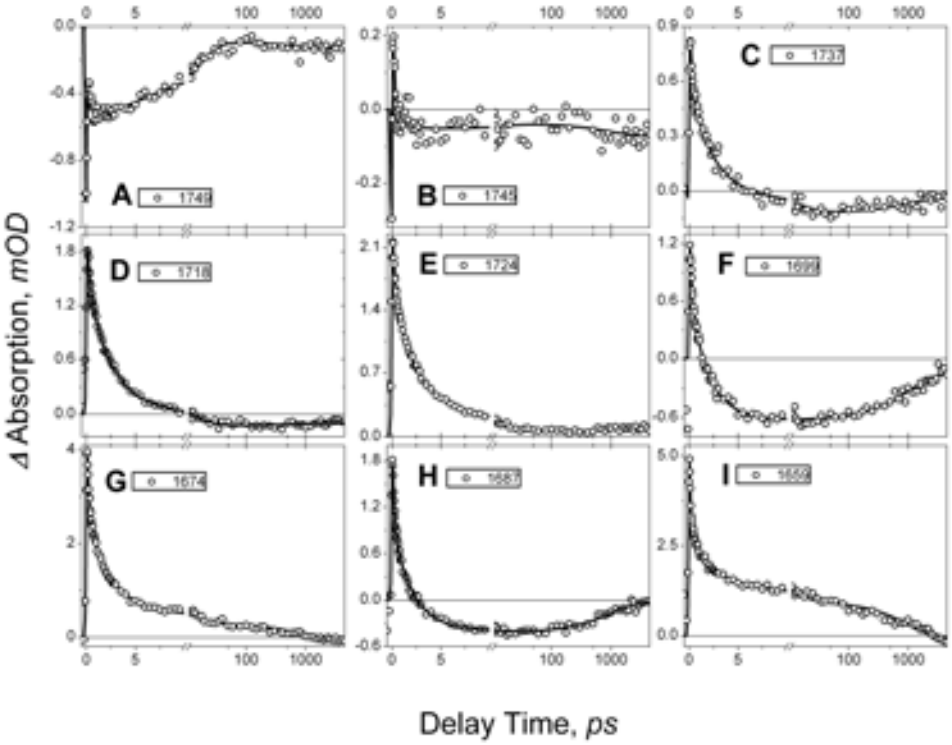

Figure 7: Nine selected time traces relative to the 480 nm data are reported. The time axis is linear between zero and ten picoseconds and logarithmic thereafter.

10a-esters at 1749(-) and 1737(-) cm^{-1} (Figure 7A and C; Table 2). The absorption at 1728 cm^{-1} and the bleach at 1717 cm^{-1} (Figure 7D) are assigned to a contribution by peridinin lactone modes, possibly resulting from excitonic coupling between Chl-*a* and peridinin [53, 55].

The $^{hot}S_1^*$ state (Figure 6, bold black line) decays in 150 fs to populate vibrationally relaxed $^{cold}S_1^*$, ICT and Chl-*a* (Q_y^*). Interpretation of the SADS of the $^{hot}S_1^*$state should be conducted with some caution as perturbed FID signals may still contribute to the signals at these early times. The $^{hot}S_1^*$ SADS is characterized by a broad, nonspecific absorption extending over the entire probed spectral window with specific bleach and induced absorption bands superimposed, as observed for peridinin in solution (Figure 2 and ref [44]). The broad absorption renders the assignment of specific bleach and induced absorptions difficult. However, from the literature the negative-going bands can be assigned (a list of band positions and interpretations is given in Table 2):

Table 2 Spectral positions and assignments of the observed vibratonal bands in the SADS that follow from target analysis on femtosecond time-resolved transient absorption data of PCP domain after exciting the Per with a 480 nm laser pulse. See Figure 5 and 6, and text for details

S_2	$^{hot}S_1$*	ICT	$^{cold}S_1$*	Q_y*	^{3}[PCP]	
1749(-)	1749(-) 1740(+ sh)		1750(-) 1740(+ sh)	1749(-)	1749(-)	Lactone *10a*-ester
		1745(-)				Lactone
1724(+)	1724(+)	1728(+)	1728(+)	1737(-) 1728(+)	1737(- sh) 1725(+)	Lactone *10a*-ester
1717(-) 1708(+)	1706(+)	1710(+)	1712(+)	1717(-)	1717(-)	Lactone
1699(-)	1699(-) 1676(+ sh)	1699 (-) 1680(+)	1699 (-) 1674(+ sh)	1699 (-)	1701(-)	*9*-keto *Per*
1659(+)	1687(-) 1666(+)	1687(-) 1664(+)	1687(-)	1687(-) 1659(+)	1687(-)	*9*-keto *Per*

the bands at 1749 and 1720 cm^{-1} originate from the peridinin lactone carbonyl [41] (Papagiannakis and Robert, unpublished). The negative-going bands at 1699 and 1687 cm^{-1} can clearly be assigned to the *9*-keto of Chl-*a* (Figure 3 and [45]). Assigning the positive-going features in this

SADS is awkward because one cannot *a priori* distinguish a bleach/induced absorption (band shift) feature from a bleach superimposed on a broad background. This is especially true for $^{hot}S_1^*$ because its short lifetime (150 fs) will result in a significant line broadening of the vibrationally excited modes by ~30 cm^{-1}.

The peridinin $^{cold}S_1^*$ state is directly formed by the decay of $^{hot}S_1^*$. The $^{cold}S_1^*$ SADS (bold dark gray line) is characterized by a prominent bleach at 1750 cm^{-1} that can readily be assigned to the Per lactone carbonyl. Strikingly, the amplitude of this band is much larger than that observed in peridinin in solution, where only a small dip on an otherwise broad absorption is observed in this region (Figure 2, ref.[44]). This implies that when bound to PCP, the oscillator strength of the peridinin lactone carbonyl is much higher than in organic solvent, or that in solution the lactone bleach is largely compensated by induced absorption in the transient IR spectrum. The S_1 SADS has a broad, rather featureless absorption from 1740 to 1650 cm^{-1}, with negative-going dips at 1700 and 1685 cm^{-1}. These dips are at a position similar to that of the Chl-*a* 9-keto' s in the Chl-*a* and $^{hot}S_1^*$ SADS, but are less resolved. In fact, peridinin in chloroform (Figure 2A) shows similar dips at 1705 and 1685 cm^{-1} suggesting that they are, at least partly, intrinsic to the peridinin S_1 state. Notably, the S_1 SADS shows signatures of vibrational cooling when compared to the $^{hot}S_1^*$ SADS with an upshift of absorption features from 1724 to 1728 cm^{-1}, from 1706 to 1710 cm^{-1} and 1724 to 1730 cm^{-1} (see Table 2).

The peridinin ICT state is also directly populated from $^{hot}S_1^*$. The ICT state represents the main energy transfer channel to Chl-*a* at a rate of $(2\ ps)^{-1}$. Its SADS (bold light gray line) shows an overall pattern similar to that of S_1, but differs in a number of important aspects. Foremost, it shows a lactone carbonyl bleach at 1745 cm^{-1}, which is downshifted by 5 cm^{-1} with respect to $^{hot}S_1^*$ and S_1. As compared to the $^{hot}S_1^*$ SADS (which primarily feeds into ICT), the lactone down-shift suggests that the peridinin(s) in the ICT state were not initially excited by the 480 nm excitation pulse and become populated in 150 fs through peridinin-peridinin energy transfer. However, the interpretation is complicated by a possible contribution by perturbed FID signals. The downshift of the lactone mode in the ground state may be due to a more polar environment of this particular (pool of) peridinin(s), which in turn promotes the intramolecular charge-transfer character of peridinin upon

excitation. In the ICT SADS, as for $^{hot}S_1^*$, the negative-going doublet at 1699 cm and 1687 cm^{-1} is observed, assigned to the Chl-*a* *9*-keto vibrations (cf. Figure 3 and the thin black Chl-*a* SADS in Figure 6). Although this feature is similar to the dip in the absorption at these frequencies observed in the S_1 state (Figure 6, thin dark gray), the resolved double peaks likely indicate involvement of the Chl-*a* *9*-keto vibrations in this SADS.

The ^{3}[PCP]* triplet SADS, (bold dark gray line), is associated with the long-lived triplet state in PCP. Like for 660 nm excitation, this SADS shows contributions from both Per and Chl-*a*. The *9*-keto bleach vibrations are visible at 1701 cm^{-1} (Chl-*a* 601) and 1687 cm^{-1} (Chl-*a* 602). The peridinin lactone C=O stretch contributions are present with bands at 1749(-)/1725(+) cm^{-1} (with a shoulder at 1737(-) cm^{-1} assigned to *10a*-ester of Chl-*a* 601) and at 1717(-) cm^{-1}. As for the 660 nm excitation, the Peridinin signals found in the Q_y^* spectrum are assigned to ^{3}[Per]*, the bleach associated with the *9*-keto of Chlorophyll 601 at 1700 cm^{-1}, are assigned to ^{3}[Chl-*a*]*. The observation of coexisting ^{3}[Per]* and ^{3}[Chl-*a*]* features in the PCP triplet spectrum is consistent with the observations with time-resolved FTIR spectroscopy, and assigned to a triplet state delocalized between peridinin and Chl-*a* [47, 56].

Discussion

The mid-IR signatures of excited peridinin and Chl-*a*

By applying a target analysis to the time-resolved mid-IR data, we have determined the IR signatures of the various molecular states that transiently exist during the excited-state energy transfer and relaxation processes in PCP. It is particularly interesting to compare the IR spectra of peridinin in the S_1 state and in the ICT state, as these states have distinct properties, in solution as well as bound to PCP [5, 15, 21, 25, 53]. In the visible, the ICT state is characterized by an excited-state absorption that is significantly red-shifted with respect to that of S_1, and by the presence of a pronounced emission in the near-IR [21, 25]. In the mid-IR, however, the S_1 and ICT states do not exhibit distinctly different spectral features when bound to PCP. Apart from different lactone

frequencies, the induced absorption patterns are similar with a broad, nonspecific absorption ranging from 1760 to 1660 cm^{-1} (Figure 6). This observation agrees with our results on peridinin in solution (Figure 2A,B) and those of Van Tassle *et al* : excitation of peridinin in a polar or nonpolar solvent gives rise to IR spectra of ICT and S_1 states that are very similar (Figure 2 and ref. [44]). Thus, even if a peridinin structural change accompanies the separate relaxation pathways into the S_1 and ICT states [24], such putative changes remain minor to the extent that the IR spectrum does not change noticeably. The downshift of the lactone mode in the peridinin ICT state may result from a more polar environment of these particular peridinins, which in turn promotes formation of the ICT state upon excitation by lowering the energy of the CT state.

It was previously observed that excitation of Chl-*a* in PCP results in a prompt bleach signal at 530 nm, assigned to excitonic or charge-transfer coupling between peridinin and Chl-*a* [53, 55]. For singlet-excited Chl-*a*, we observe a 1720 cm^{-1} bleach feature which may be assigned to a peridinin lactone (Figure 6, thin black line). It also shows a bleach at 1750 cm^{-1} that either belongs to Chl-*a 10a*-ester or a peridinin lactone. Ultrafast polarized visible spectroscopy has shown that most likely, Per624/614 are responsible for the prompt bleach at 530 nm [53, 55]. Thus, Per624/614 have their lactone frequencies at 1720 cm^{-1} and, possibly, at 1750 cm^{-1}, as will be substantiated below.

In the SADS assigned to excited-state peridinin, distinct contributions from Chl-*a* are observed. In the $^{hot}S_1^*$ and ICT states, clear Chl-*a 9*-keto bleaches are observed at 1699 and 1685 cm^{-1} (Figure 6, black and bold light gray curves). On the other hand, the peridinin $^{cold}S_1^*$ state does not exhibit an obvious Chl-*a 9*-keto signal. This observation suggests that the strong electric field generated by the ICT state and its precursor, $^{hot}S_1^*$, induces a vibrational Stark effect on the Chl-*a 9*-keto modes, causing them to shift frequency or to lose oscillator strength. The peridinin S_1 state does not, or to a less extent exhibit a charge-transfer character, which explains the absence of a Chl-*a 9*-keto signal in its SADS. Note that the initially excited peridinin S_2 state possesses a large charge-transfer character [57] which makes it reasonable to assume that $^{hot}S_1^*$ does so as well. We previously reported that the IR spectrum of the PCP triplet state bears features of both peridinin triplet as Chl-*a* triplet states, which we assigned to delocalization of the wavefunction among peridinin and Chl-*a* [47, 56]. For the peridinin singlet excited state, such

wavefunction mixing or an excitonic interaction is not required to explain the appearance of Chl-*a* features in its SADS.

Identification of energy transfer pathways in PCP

The ultrafast IR experiments on PCP provide for a unique opportunity to identify site-specific energy transfer processes through the lactone frequencies of particular peridinins. A most striking aspect that immediately follows from the target analysis presented in Figure 6 is the observation that the lactone frequency of the peridinin carrying the ICT state (1745 cm^{-1}, bold light gray line) is markedly different from the peridinin carrying the triplet state (1749 cm^{-1}, bold dark gray line). This observation implies that the main singlet and triplet energy transfer pathways in the PCP complex are distinct. Overall, we can identify three bleaches associated with peridinin lactone in PCP: 1749, 1745 and 1717 cm^{-1}. These frequencies fairly agree with those observed on the microsecond timescale with step-scan FTIR spectroscopy, where lactone bleaches were found at 1745, 1741 and 1720 cm^{-1}. Resonant Raman on PCP excited at 476 nm reveals two broad bands at 1745 and 1723 cm^{-1} with a shoulder at 1742 cm^{-1} (E. Papagiannakis and B. Robert, unpublished data). In the following, we will identify singlet and triplet energy transfer pathways in PCP on the basis of the observed peridinin lactone frequencies and assign them to the particular peridinins.

In the triplet state, the main lactone bleach is found at 1749 cm^{-1} (Figure 6, bold dark gray line) and at 1745 cm^{-1} by Alexandre *et al* [47]. The slight discrepancy of ~4 cm^{-1} falls within the spectral resolution of the experiments (6 cm^{-1} here and 8 cm^{-1} in [47]) and the uncertainties in the calibration procedure of the femtosecond IR apparatus. Recently, Carbonera and co-workers identified Per624/614 as the main acceptor of Chl-*a* triplets [58, 59]. Given that triplet-triplet migration among the peridinins is unlikely to occur in the PCP complex [58], it is fair to state that the main lactone bleaches in the femto-IR (1749 cm^{-1}) and step-scan FTIR (1745 cm^{-1}) experiments represent the same peridinin pair, identified as Per624/614. In addition, a smaller bleach in the triplet state is observed at 1720 cm^{-1}, indicating a fraction or subpopulation of Per624/614 with a downshifted lactone frequency.

The slowly-transferring peridinin S_1 state has a minor contribution to the total energy transfer process to Chl-*a*. It has its lactone frequency at 1749 cm^{-1} (thin dark gray in Figure 6). Per622/612 were proposed earlier to carry the slowly-transferring S_1 state [53]. At this point it is of interest to recall the properties of the the so-called high-salt PCP complex (HSPCP). HSPCP appears as a minor fraction in the PCP isolation procedure and slightly differs from main-form PCP (referred to as PCP in this manuscript) in amino acid composition, molar mass, antigenicity, absorption and fluorescence properties [60]. The single most important structural difference between high-salt PCP and main-form PCP is that Per622/612 are absent in the former complex. Most interestingly, the peridinin-to- Chl-*a* energy transfer dynamics are essentially the same in high-salt PCP as compared to main-form PCP [61, 62]. Thus, Per622/612 almost certainly carry the S_1 state, representing the slow, minor energy transfer pathway to Chl-*a*.

In PCP, the peridinin ICT state represents the main excited-state energy donor to Chl-*a*. The peridinins carrying the ICT state have their lactone frequency at 1745 cm^{-1}. This sets them apart from the peridinins carrying the S_1 and triplet states, which have their lactones at 1749 cm^{-1}. As the latter have been identified as Per622/612 and Per624/614, respectively, it follows that the ICT state localizes mainly on Per621/611 and/or Per623/613.

Overall, the excited-state energy transfer and relaxation pathways in PCP can be summarized as follows: upon excitation of peridinin in its main band at 480 nm, exciton relaxation among the strongly coupled peridinins may take place in the S_2 state [63] prior to internal conversion to low-lying peridinin excited states and a ~25% fraction of energy transfer to Chl-*a*. These excitation conditions preferentially lead to population of Per622/612, Per621/611 and Per623/613, whereas the Per624/614 pair becomes hardly populated. After relaxation from the S_2^* state, Per621/611 and Per623/613 evolve into the low-lying ICT state which is promoted by a more polar environment and constitute the main energy transfer channel to Chl-*a*. Per622/612 evolve into the S_1 state and are weakly coupled to Chl-*a*, representing a minor fraction of energy transfer to Chl-*a* with a lifetime of 12 ps. After excited-state energy transfer to Chl-*a* is complete, intersystem crossing to the Chl-*a* triplet state takes place, followed by triplet-triplet energy transfer to Per624/614. The latter process is rate-limited by the Chl-*a* singlet-excited state

lifetime. Thus, our observations imply that upon excitation at 480 nm, singlet and triplet energy transfer pathways are to a significant extent separated.

Acknowledgements

C.B. was supported by the Life Sciences Councel of the Netherlands Organization for Scientific Research (NWO-ALW). M.T.A.A was supported by NWO-ALW through the 'Molecule to Cell' programme. J.T.M.K. was supported by NWO-ALW through a VIDI fellowship.

References

1. Sundstrom V, Pullerits T, van Grondelle R: **Photosynthetic Light-Harvesting: Reconciling Dynamics and Structure of Purple Bacterial LH2 Reveals Function of Photosynthetic Unit.** *Journal of Physical Chemistry B* 1999, **103**(13):2327-2346.
2. van Amerongen H, van Grondelle R: **Understanding the Energy Transfer Function of LHCII, the Major Light-Harvesting Complex of Green Plants.** *Journal of Physical Chemistry B* 2001, **105**(3):604-617.
3. Gradinaru CC, Kennis JT, Papagiannakis E, van Stokkum IH, Cogdell RJ, Fleming GR, Niederman RA, van Grondelle R: **An unusual pathway of excitation energy deactivation in carotenoids: singlet-to-triplet conversion on an ultrafast timescale in a photosynthetic antenna.** *Proc Natl Acad Sci U S A* 2001, **98**(5):2364-2369.
4. Papagiannakis E, Kennis JT, van Stokkum IHM, Cogdell RJ, van Grondelle R: **An alternative carotenoid-to-bacteriochlorophyll energy transfer pathway in photosynthetic light harvesting.** *Proc Natl Acad Sci U S A* 2002, **99**(9):6017-6022.
5. Polivka T, Sundstrom V: **Ultrafast dynamics of carotenoid excited States-from solution to natural and artificial systems.** *Chem Rev* 2004, **104**(4):2021-2071.
6. Ritz T, Damjanovic A, Schulten K, Zhang JP, Koyama Y: **Efficient light harvesting through carotenoids.** *Photosynth Res* 2000, **66**(1-2):125-144.

7. Field CB, Behrenfeld MJ, Randerson JT, Falkowski P: **Primary production of the biosphere: integrating terrestrial and oceanic components.** *Science* 1998, **281**(5374):237-240.
8. Apt KE, Collier JL, Grossman AR: **Evolution of the phycobiliproteins.** *J Mol Biol* 1995, **248**(1):79-96.
9. Macpherson AN, Hiller RG: **Light-Harvesting Antennas in Photosynthesis**, vol. 13: Springer; 2003.
10. Mimuro M, Tamai N, Ishimaru T, Yamazaki I: **Characteristic Fluorescence Components in Photosynthetic Pigment System of a Marine Dinoflagellate, Protogonyaulax-Tamarensis, and Excitation-Energy Flow among Them - Studies by Means of Steady-State and Time-Resolved Fluorescence Spectroscopy.** *Biochim Biophys Acta* 1990, **1016**(2):280-287.
11. Knoetzel J, Rensing L: **Characterization of the Photosynthetic Apparatus from the Marine Dinoflagellate Gonyaulax-Polyedra .2. Circadian Rhythmicity of Photosynthesis and the Supramolecular Organization of Pigment-Protein Complexes.** *J Plant Physiol* 1990, **136**(3):280-288.
12. Hofmann E, Wrench PM, Sharples FP, Hiller RG, Welte W, Diederichs K: **Structural basis of light harvesting by carotenoids: peridinin-chlorophyll-protein from Amphidinium carterae.** *Science* 1996, **272**(5269):1788-1791.
13. Holt NE, Kennis JTM, Fleming GR: **Femtosecond fluorescence upconversion studies of light harvesting by beta-carotene in oxygenic photosynthetic core proteins.** *J Phys Chem B* 2004, **108**(49):19029-19035.
14. Holt NE, Kennis JTM, Dall'Osto L, Bassi R, Fleming GR: **Carotenoid to chlorophyll energy transfer in light harvesting complex II from Arabidopsis thaliana probed by femtosecond fluorescence upconversion.** *Chem Phys Lett* 2003, **379**(3-4):305-313.
15. Bautista JA, Hiller RG, Sharples FP, Gosztola D, Wasielewski M, Frank HA: **Singlet and triplet energy transfer in the peridinin-chlorophyll a protein from Amphidinium carterae.** *Journal of Physical Chemistry A* 1999, **103**(14):2267-2273.
16. Krueger BP, Lampoura SS, van Stokkum IHM, Papagiannakis E, Salverda JM, Gradinaru CC, Rutkauskas D, Hiller RG, van Grondelle R: **Energy transfer in the peridinin chlorophyll-a protein of Amphidinium carterae studied by polarized transient absorption and target analysis.** *Biophys J* 2001, **80**(6):2843-2855.
17. Song PS, Koka P, Prezelin BB, Haxo FT: **Molecular topology of the photosynthetic light-harvesting pigment complex, peridinin-chlorophyll a-protein, from marine dinoflagellates.** *Biochemistry* 1976, **15**(20):4422-4427.

18. Kleima FJ, Hofmann E, Gobets B, van Stokkum IHM, van Grondelle R, Diederichs K, van Amerongen H: **Forster excitation energy transfer in peridinin-chlorophyll-a-protein**. *Biophysical Journal* 2000, **78**(1):344-353.
19. Bautista JA, Connors RE, Raju BB, Hiller RG, Sharples FP, Gosztola D, Wasielewski MR, Frank HA: **Excited State Properties of Peridinin: Observation of a Solvent Dependence of the Lowest Excited Singlet State Lifetime and Spectral Behavior Unique among Carotenoids**. *JPhysChem B* 1999, **103**(41):8751-8758.
20. Polivka T, Hiller RG, Frank HA: **Spectroscopy of the peridinin-chlorophyll-a protein: Insight into light-harvesting strategy of marine algae**. *Archives of Biochemistry and Biophysics* 2007, **458**(2):111-120.
21. Zigmantas D, Hiller RG, Sundstr ö m V, Pol í vka T: **Carotenoid to chlorophyll energy transfer in the peridinin – chlorophyll- a – protein complex involves an intramolecular charge transfer state**. *Proc Natl Acad Sci USA 99* 2002, **99**(26):16760-16765.
22. Frank HA, Bautista JA, Josue J, Pendon Z, Hiller RG, Sharples FP, Gosztola D, Wasielewski MR: **Effect of the Solvent Environment on the Spectroscopic Properties and Dynamics of the Lowest Excited States of Carotenoids**. *JPhysChem B* 2000, **104**(18):4569-4577.
23. Papagiannakis E, Larsen DS, van Stokkum IHM, Vengris M, Hiller RG, van Grondelle R: **Resolving the excited state equilibrium of peridinin in solution**. *Biochemistry* 2004, **43**(49):15303-15309.
24. Zigmantas D, Hiller RG, Yartsev A, Sundstr ö m V, Pol í vka T: **Dynamics of Excited States of the Carotenoid Peridinin in Polar Solvents: Dependence on Excitation Wavelength, Viscosity, and Temperature**. *JPhysChem B* 2003, **107**(22):5339-5348.
25. Zigmantas D, Pol í vka T, Hiller RG, Yartsev A, Sundstr ö m V: **Spectroscopic and Dynamic Properties of the Peridinin Lowest Singlet Excited States**. *JPhysChem A* 2001, **105**(45):10296-10306.
26. Krikunova M, Lokstein H, Leupold D, Hiller RG, Voigt B: **Pigment-pigment interactions in PCP of Amphidinium carterae investigated by nonlinear polarization spectroscopy in the frequency domain**. *Biophys J* 2006, **90**(1):261-271.
27. Groot ML, van Wilderen LJGW, Di Donato M: **Time-resolved methods in biophysics. 5. Femtosecond time-resolved and dispersed infrared spectroscopy on proteins**. *Photochemical and Photobiological Sciences* 2007, **6**(5):501-507.
28. Kotting C, Gerwert K: **Proteins in action monitored by time-resolved FTIR spectroscopy**. *Chemphyschem* 2005, **6**(5):881-888.
29. Di Donato M, van Grondelle R, van Stokkum IHM, Groot ML:

Excitation energy transfer in the Photosystem II core antenna complex CP43 studied by femtosecond visible/visible and visible/mid-infrared pump probe spectroscopy. *J Phys Chem B* 2007, **111**(25):7345-7352.

30. Groot ML, Breton J, van Wilderen LJGW, Dekker JP, van Grondelle R: **Femtosecond visible/visible and visible/mid-IR pump-probe study of the photosystem II core antenna complex CP47**. *Journal of Physical Chemistry B* 2004, **108**(23):8001-8006.
31. Groot ML, Pawlowicz NP, van Wilderen L, Breton J, van Stokkum IHM, van Grondelle R: **Initial electron donor and acceptor in isolated Photosystem II reaction centers identified with femtosecond mid-IR spectroscopy**. *Proc Natl Acad Sci U S A* 2005, **102**(37):13087-13092.
32. Di Donato M, Cohen RO, Diner BA, Breton J, van Grondelle R, Groot ML: **Primary charge separation in the photosystem II core from Synechocystis: A comparison of femtosecond visible/midinfrared pump-probe spectra of wild-type and two P-680 mutants**. *J Phys Chem B* 2008, **94**(12):4783-4795.
33. Pawlowicz NP, Van Grondelle R, van Stokkum IHM, Breton J, Jones MR, Groot ML: **Identification of the first steps in charge separation in bacterial photosynthetic reaction centers of Rhodobacter sphaeroides by ultrafast mid-infrared spectroscopy: Electron transfer and protein dynamics**. *Biophys J* 2008, **95**(3):1268-1284.
34. Pawlowicz NP, Groot ML, van Stokkum IHM, Breton J, van Grondelle R: **Charge separation and energy transfer in the photosystem II core complex studied by femtosecond midinfrared spectroscopy**. *Biophys J* 2007, **93**(8):2732-2742.
35. Herbst J, Heyne K, Diller R: **Femtosecond infrared spectroscopy of bacteriorhodopsin chromophore isomerization**. *Science* 2002, **297**(5582):822-825.
36. Heyne K, Mohammed OF, Usman A, Dreyer J, Nibbering ET, Cusanovich MA: **Structural evolution of the chromophore in the primary stages of trans/cis isomerization in photoactive yellow protein**. *Journal of the American Chemical Society* 2005, **127**(51):18100-18106.
37. van Thor JJ, Ronayne KL, Towrie M: **Formation of the early photoproduct Lumi-R of cyanobacterial phytochrome Cph1 observed by ultrafast mid-infrared spectroscopy**. *Journal of the American Chemical Society* 2007, **129**(1):126-132.
38. Kennis JTM, Groot ML: **Ultrafast spectroscopy of biological photoreceptors**. *Curr Opinion Struct Biol* 2007, **17**(5):623-630.
39. Bonetti C, Mathes T, van Stokkum IHM, Mullen KM, Groot ML, van Grondelle R, Hegemann P, Kennis JTM: **Hydrogen Bond Switching**

among Flavin and Amino Acid Side Chains in the BLUF Photoreceptor Observed by Ultrafast Infrared Spectroscopy. *Biophysical Journal* 2008, **95**(10):4790-4802.

40. van Wilderen LJGW, van der Horst MA, van Stokkum IHM, Hellingwerf KJ, van Grondelle R, Groot ML: **Ultrafast infrared spectroscopy reveals a key step for successful entry into the photocycle for photoactive yellow protein.** *Proc Natl Acad Sci U S A* 2006, **103**(41):15050-15055.
41. Martinson TA, Plumley FG: **One-step extraction and concentration of pigments and acyl lipids by sec-butanol from in vitro and in vivo samples.** *Analytical biochemistry* 1995, **228**(1):123-130.
42. van Stokkum IHM, Larsen DS, van Grondelle R: **Global and target analysis of time-resolved spectra.** *Biochim Biophys Acta* 2004, **1657**(2-3):82-104.
43. Mullen KM, van Stokkum IHM: **TIMP: An R package for modeling multi-way spectroscopic measurements.** *Journal of Statistical Software* 2007, **18**(3).
44. Van Tassle AJ, Prantil MA, Hiller RG, Fleming GR: **Excited state structural dynamics of the charge transfer state of peridinin.** *Israel J Chem* 2007, **47**(1):17-24.
45. Kleima FJ, Wendling M, Hofmann E, Peterman EJG, van Grondelle R, van Amerongen H: **Peridinin chlorophyll a protein: Relating structure and steady-state spectroscopy.** *Biochemistry* 2000, **39**(17):5184-5195.
46. Feiler U, Mattioli TA, Katheder I, Scheer H, Lutz M, Robert B: **Effects of Vinyl Substitutions on Resonance Raman-Spectra of (Bacterio)Chlorophylls.** *Journal of Raman Spectroscopy* 1994, **25**(5):365-370.
47. Alexandre MTA, Luhrs DC, van Stokkum IHM, Hiller R, Groot ML, Kennis JTM, van Grondelle R: **Triplet state dynamics in peridinin-chlorophyll-a-protein: A new pathway of photoprotection in LHCs?** *Biophysical Journal* 2007, **93**(6):2118-2128.
48. Hamm P: **Coherent Effects in femtosecond Infrared Spectroscopy.** *Chem Phys* 1995, **200**:415-429.
49. Berera R, Herrero C, van Stokkum IHM, Vengris M, Kodis G, Palacios RE, van Amerongen H, van Grondelle R, Gust D, Moore TA *et al*: **A simple artificial light-harvesting dyad as a model for excess energy dissipation in oxygenic photosynthesis.** *Proc Natl Acad Sci U S A* 2006, **103**(14):5343-5348.
50. Berera R, van Stokkum IHM, Kodis G, Keirstead AE, Pillai S, Herrero C, Palacios RE, Vengris M, van Grondelle R, Gust D *et al*: **Energy transfer, excited-state deactivation, and exciplex formation**

in artificial caroteno-phthalocyanine light-harvesting antennas. *J Phys Chem B* 2007, **111**(24):6868-6877.

51. Kodis G, Herrero C, Palacios R, Marino-Ochoa E, Gould S, de la Garza L, van Grondelle R, Gust D, Moore TA, Moore AL *et al*: **Light harvesting and photoprotective functions of carotenoids in compact artificial photosynthetic antenna designs.** *J Phys Chem B* 2004, **108**(1):414-425.
52. Polivka T, Zigmantas D, Sundstrom V, Formaggio E, Cinque G, Bassi R: **Carotenoid S(1) state in a recombinant light-harvesting complex of Photosystem II.** *Biochemistry* 2002, **41**(2):439-450.
53. van Stokkum IHM, Papagiannakis E, Vengris M, Salverda JM, Polivka T, Zigmantas D, Larsen DS, Lampoura SS, Hiller RG, van Grondelle R: **Inter-pigment interactions in the peridinin chlorophyll protein studied by global and target analysis of time-resolved absorption spectra.** *Chem Phys* 2008, **in press.**
54. Linden PA, Zimmermann J, Brixner T, Holt NE, Vaswani HM, Hiller RG, Fleming GR: **Transient Absorption Study of Peridinin and Peridinin-Chlorophyll a-Protein after Two-Photon Excitation.** *Journal of Physical Chemistry B* 2004, **108**(29):10340-10345.
55. Salverda JM: Amsterdam: Vrije Universiteit; 2003.
56. Bonetti C, Alexandre MTA, Hiller RG, J.T.M. K, van Grondelle R: **Chl-a triplet quenching by peridinin in H-PCP and organic solvent revealed by step-scan FTIR time-resolved spectroscopy.** *Chem Phys* 2008, **in press.**
57. Premvardhan L, Papagiannakis E, Hiller RG, van Grondelle R: **The charge-transfer character of the S-0 -> S-2 transition in the carotenoid peridinin is revealed by stark spectroscopy.** *Journal of Physical Chemistry B* 2005, **109**(32):15589-15597.
58. Di Valentin M, Ceola S, Salvadori E, Agostini G, Carbonera D: **Identification by time-resolved EPR of the peridinins directly involved in chlorophyll triplet quenching in the peridinin-chlorophyll a-protein from Amphidinium carterae.** *Biochimica et Biophysica Acta (BBA) - Bioenergetics* 2008, **1777**(2):186-195.
59. Di Valentin M, Ceola S, Salvadori E, Agostini G, Giacornetti GM, Carbonera D: **Spectroscopic properties of the peridinins involved in chlorophyll triplet quenching in high-salt peridinin-chlorophyll a-protein from Amphidinium carterae as revealed by optically detected magnetic resonance, pulse EPR and pulse ENDOR spectroscopies.** *Biochimica et Biophysica Acta (Bioenergetics)* 2008, **1777**(10):1355-1363.
60. Sharples FP, Wrench PM, Ou KL, Hiller RG: **Two distinct forms of the peridinin-chlorophyll alpha-protein from Amphidinium carterae.** *Biochimica et Biophysica Acta (Bioenergetics)* 1996, **1276**(2):117-

123.
61. Ilagan RP, Koscielecki JF, Hiller RG, Sharples FP, Gibson GN, Birge RR, Frank HA: **Femtosecond time-resolved absorption spectroscopy of main-form and high-salt peridinin-chlorophyll a-proteins at low temperatures**. *Biochemistry* 2006, **45**(47):14052-14063.
62. Ilagan RP, Shima S, Melkozernov A, Lin S, Blankenship RE, Sharples FP, Hiller RG, Birge RR, Frank HA: **Spectroscopic properties of the main-form and high-salt peridinin-chlorophyll a proteins from Amphidinium carterae**. *Biochemistry* 2004, **43**(6):1478-1487.
63. Damjanovic A, Ritz T, Schulten S: **Excitation Transfer in the Peridinin-Chlorophyll-Protein of *Amphidinium carterae***. *Biophys J* 2000, **79**(4):1695-1705.

Appendix

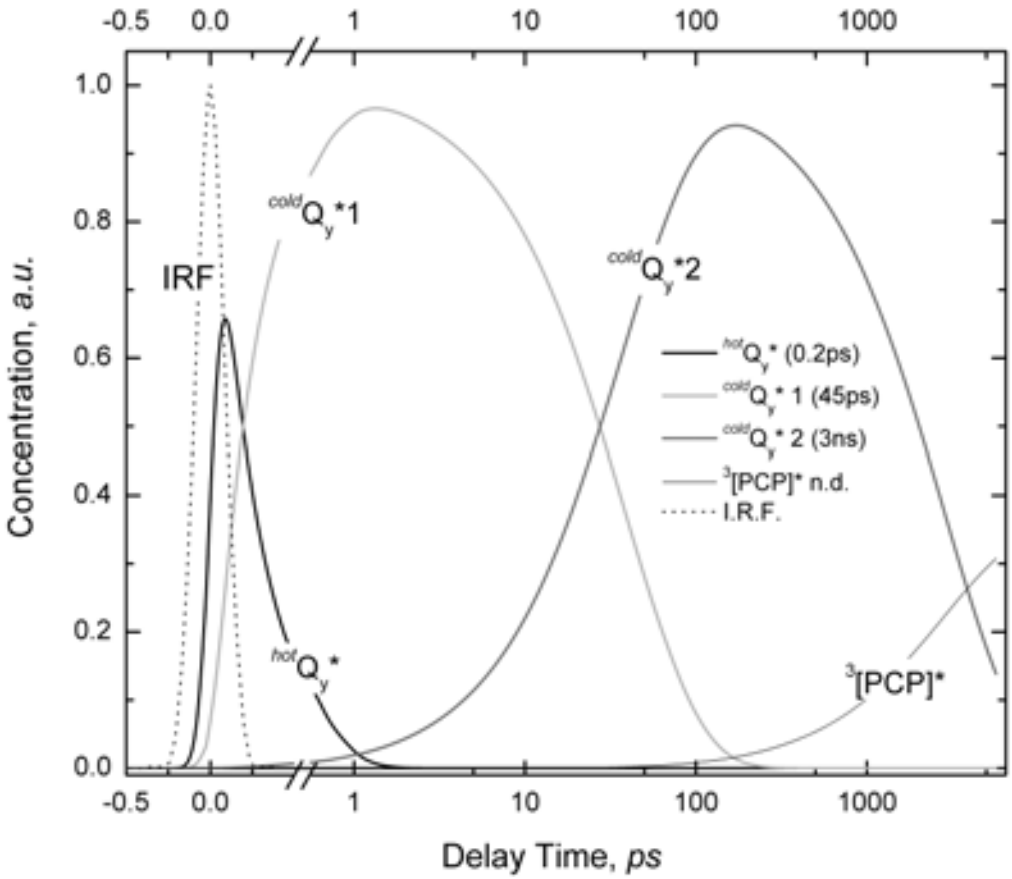

FIGURE A Concentration profiles corresponding to SADS resulting from the global analysis of the 660 nm excitation data. In the same figure is shower the IRF (150 fs).

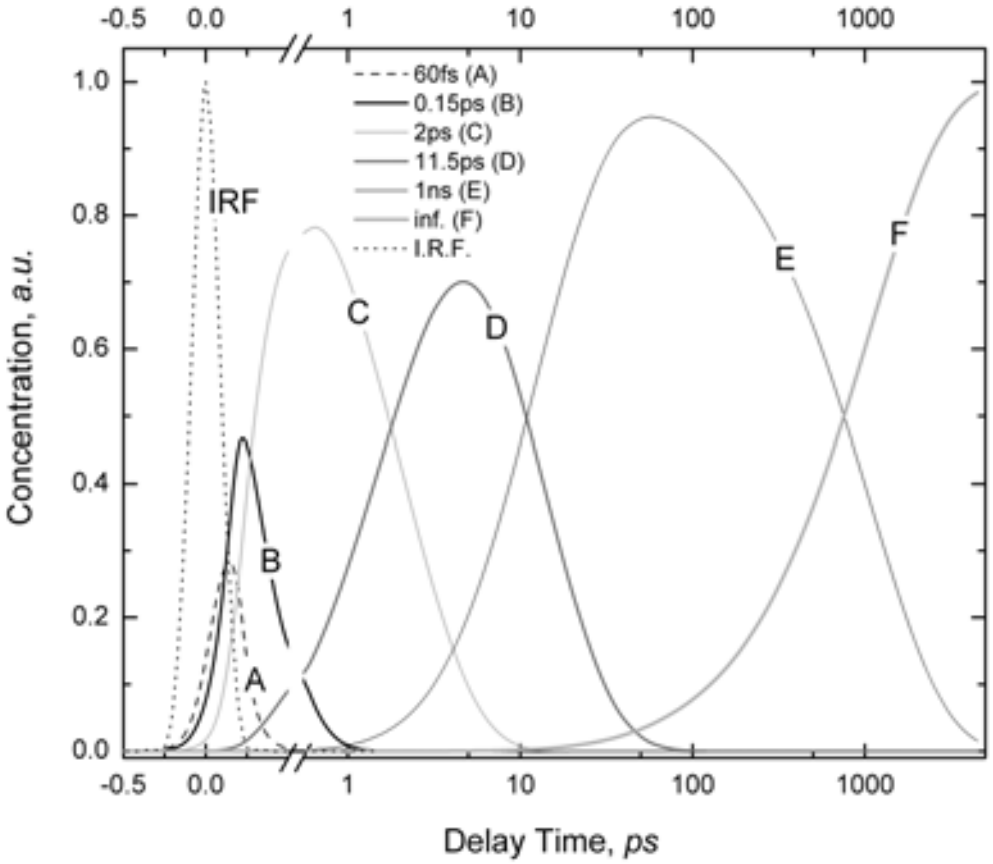

FIGURE B Concentration profiles corresponding to EADS resulting from the global analysis of the 480 nm excitation data. In the same figure is shower the IRF (150 fs).

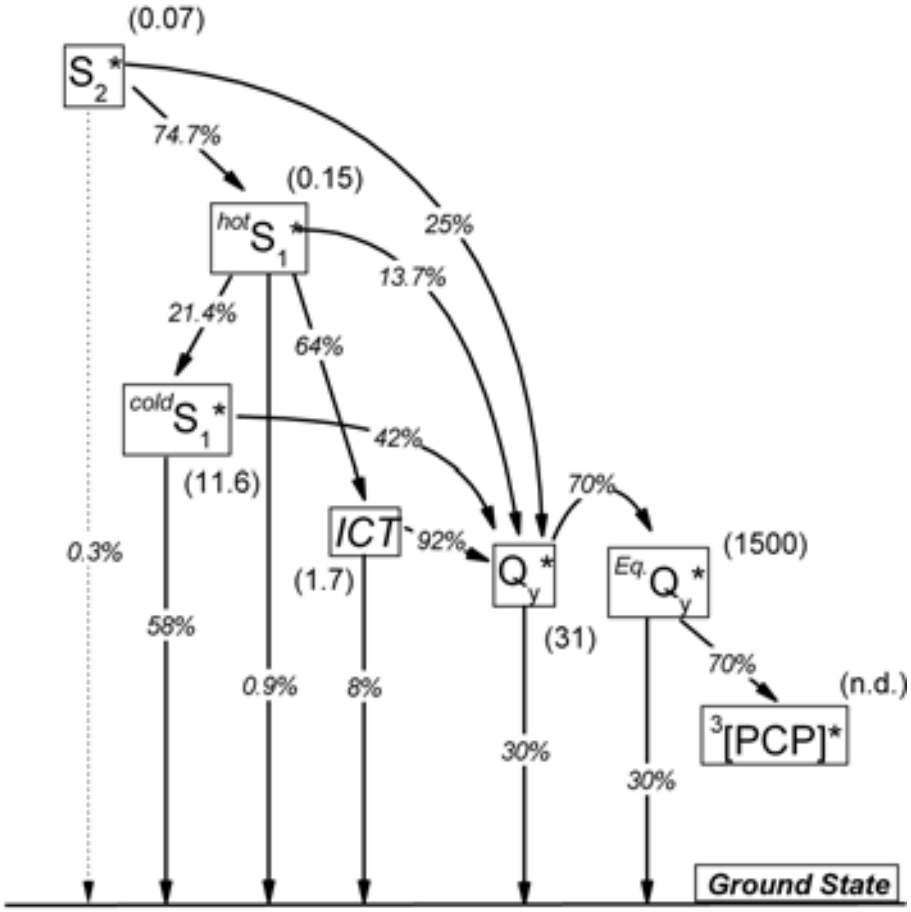

FIGURE C: Kinetic model applied for the 480 nm excitation analysis. In the scheme are drew: the connectivity among the molecular species (named inside the boxes), the life time in picosecond (brackets) for each species and the percentage of branching.

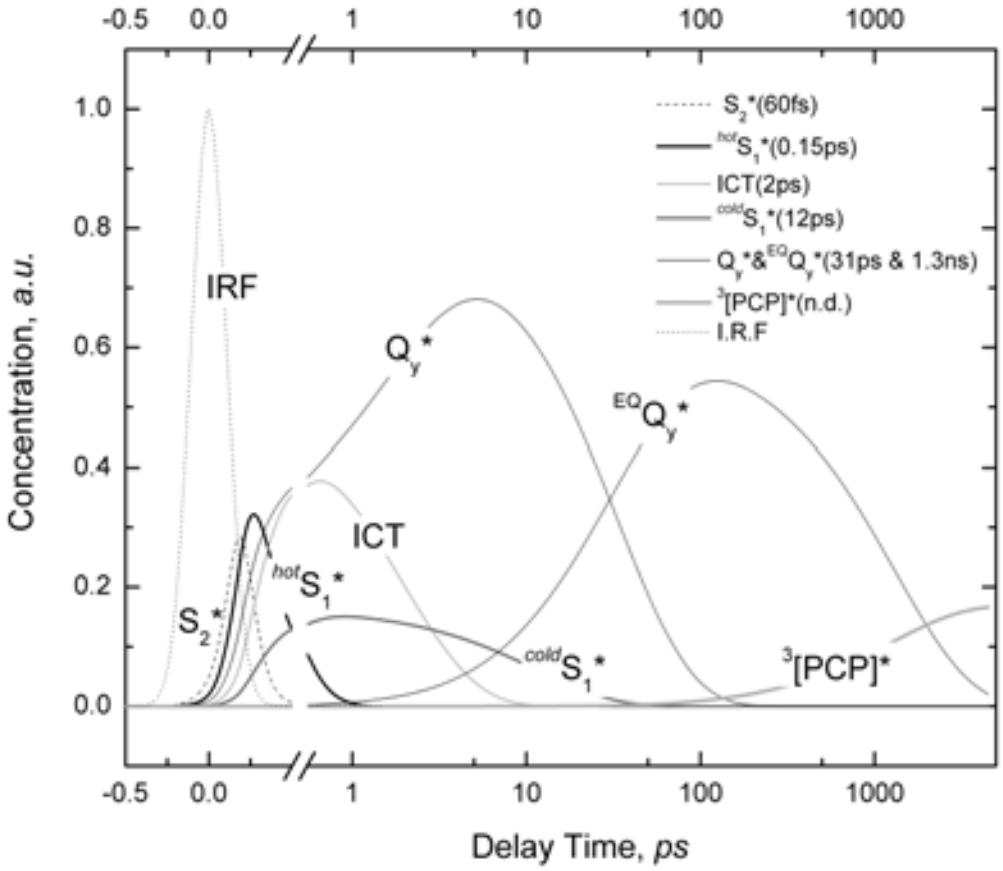

FIGURE D: Concentration profiles corresponding to SADS resulting from the global analysis of the 480 nm excitation data. In the same figure is shower the IRF (150 fs).